14th European Signal Processing Conference (EUSIPCO 2006), Florence, Italy, September 4-8, 2006, copyright by EURASIP

CONSTRUCTION OF TRIANGULAR BIORTHOGONAL WAVELET FILTERS FOR ISOTROPIC IMAGE PROCESSING

Susumu Sakakibara and Oleg V. Vasilyev

School of Information Environment, Tokyo Denki University
2-1200 Muzaigakuendai, Inzai, Chiba, Japan, 270-1382
phone: + (81) 476-46-8748, fax: + (81) 476-46-8499, email: susumu@sie.dendai.ac.jp
web: www.sie.dendai.ac.jp

Department of Mechanical Engineering, University of Colorado
ECME 126, Boulder, Co. 80309-0427
phone: +(1) 303-492-4717, email: Oleg.Vasilyev@colorado.edu

ABSTRACT

We propose new non-separable two dimensional biorthogonal wavelets whose filters are defined on the regular triangular lattice on a plane. Their construction uses lifting in the polyphase representation of the filters. While filters of arbitrary orders may be obtained by following the same way as in 1D case, in this paper we focus our attention mainly on the construction method using a few simple examples. Applying one of the example filters to simple images, we show that isotropy of images are improved in the wavelet transform as compared with the usual tensor product wavelet transform.

1. INTRODUCTION

Image processing is one of the major application areas of wavelet transform. In most cases wavelet transform is carried out in the tensor product form, i.e., one dimensional wavelet transform is applied in horizontal and vertical components of the matrices of image data independently [1]. As a result, isotropy of images may not be well respected. To remedy this drawback, many attempts have been carried out to construct non-separable wavelets [2], or to implement dual-tree wavelet transforms [3, 4]. They are not used as a standard tool, however, because they are not so easy to construct or to use in actual computations.

On the other hand, in the advent of lifting scheme [5], the so-called second generation wavelets [6] have opened a way to handle data on irregular grids over arbitrary surfaces [7]. They seem to gain popularity in efficient parametrization of curved surfaces, in the framework of subdivision scheme [8]. However, isotropy, or rotational symmetry, in two dimensional data is not of major concern.

If we restrict to data on a plane such as images, the usual (first generation) wavelets would be more desirable, since they would allow simpler computation due to their periodicity on the plane. As a first step toward this end, we propose biorthogonal wavelets whose filters are defined on the regular triangular lattice, which we call triangular wavelets.

After submission of this paper, the authors have learned of [11, 12], in which orthogonal quadrature mirror filters defined on the triangular lattice have been considered. While their results agree with ours partly, e.g., the halfband condition (7) below, our method is completely new. In fact, our method uses lifting in the polyphase representation extended to the triangular lattice, which allows construction of triangular biorthgonal wavelet filters of an arbitrary order.

After a brief review on 1D biorthogonal wavelet filtes in the next section, we explain how to construct our triangular wavelet filters, following the general formalism laid out by one of the authors for orthogonal case [13]. As a concrete example, we construct the CDF(2,2) biorthogonal filter extended to the triangular lattice, and show their structure in the frequency domain together with comparison with the features of a filter in [11]. Finally, applying the filters to some simple images, we demonstrate that isotropy of images are well respected. Section 5 summarizes our conclusions.

2. BIORTHOGONAL WAVELETS

The discrete signal $\{c_j[k]\}$, $k \in \mathbb{Z}$, is decomposed by the low pass (LP) filter $\{h[k]\}$ and the high pass (HP) filter $\{g[k]\}$, followed by downsampling, to yield the coarse component $\{c_{j-1}[k]\}$ and detail component $\{d_{j-1}[k]\}$, respectively, of half a resolution. In the polyphase representation, the signal

$$\hat{c}_j(\omega) = \sum_{k\in\mathbb{Z}} c_j[k]\, e^{-i\omega k}$$

is decomposed into even and odd components

$$\hat{c}_{j,e}(\omega) = \sum_{k\in\mathbb{Z}} c_j[2k]\, e^{-i\omega k}, \quad \hat{c}_{j,o}(\omega) = \sum_{k\in\mathbb{Z}} c_j[2k+1]\, e^{-i\omega k},$$

and the decomposition of the signal is carried out as

$$\begin{pmatrix} \hat{c}_{j-1}(2\omega) \\ \hat{d}_{j-1}(2\omega) \end{pmatrix} = \widehat{P}(2\omega)^{\dagger} \begin{pmatrix} \hat{c}_{j,e}(2\omega) \\ \hat{c}_{j,o}(2\omega) \end{pmatrix}, \tag{1}$$

where $\widehat{P}(\omega)^{\dagger}$ is the Hermitian conjugate of the polyphase matrix.

A convenient method to construct invertible polyphase matrices is lifting. The odd-indexed sample $c_j[2k+1]$ is predicted by the predictor p of even-indexed samples $c_j[2k]$, and $c_j[2k+1]$ is replaced by $d_{j-1}[k]$ which is the difference between the original value and the prediction,

$$c_j[2k+1] \to d_{j-1}[k] = c_j[2k+1] - p(c_j[2k]).$$

Then, the even-indexed samples $c_j[2k]$ are updated by

$$c_j[2k] \to c_{j-1}[k] = c_j[2k] + u(d_{j-1}[k]),$$

where the normalization of the updater u is chosen such that the sum of the coarse components is halved by the decomposition,

$$\sum_k c_{j-1}[k] = \frac{1}{2}\sum_k c_j[k].$$

Finally, $c_j[k]$ and $d_j[k]$ are rescaled by $\sqrt{2}$ and $1/\sqrt{2}$, respectively, such that the total energy of the signal is preserved by the decomposition. This scheme corresponds to the polyphase matrix

$$\widehat{P}(\omega)^\dagger = \begin{pmatrix} \sqrt{2} & 0 \\ 0 & 1/\sqrt{2} \end{pmatrix} \begin{pmatrix} 1 & \hat{u}(\omega) \\ 0 & 1 \end{pmatrix} \begin{pmatrix} 1 & 0 \\ -\hat{p}(\omega) & 1 \end{pmatrix}, \qquad (2)$$

where $\hat{p}(\omega)$ is defined by $\sum_k p(c_j[2k])e^{-i\omega k} = \hat{p}(\omega)\,\hat{c}_{j,e}(\omega)$, and similarly for the updater $\hat{u}$. This polyphase matrix is invertible, and the reconstruction is carried out by its inverse, which guarantees perfect reconstruction. In particular, if $\hat{p}$ and $\hat{u}$ are polynomials of $e^{-i\omega}$, the decomposition and reconstruction filters become FIR, with primal and dual filters, respectively.

For example, the choice $\hat{p}(\omega) = 1$ and $\hat{u}(\omega) = 1/2$ gives Haar filter, $\hat{h}(\omega) = \hat{\tilde{h}}(\omega) = (1 + e^{-i\omega})/\sqrt{2}$, and $\hat{g}(\omega) = \hat{\tilde{g}}(\omega) = (-1 + e^{-i\omega})/\sqrt{2}$, which turns out to be orthogonal. On the other hand, if we choose the linear prediction,

$$\hat{p}(\omega) = \frac{1 + e^{i\omega}}{2}, \quad \hat{u}(\omega) = \frac{1 + e^{-i\omega}}{4},$$

then we obtain the CDF (2,2) filter [9]

$$\begin{aligned} \hat{h}(\omega) &= \frac{-e^{i2\omega} + 2e^{i\omega} + 6 + 2e^{-i\omega} - e^{-i2\omega}}{4\sqrt{2}}, \\ \hat{g}(\omega) &= \frac{-1 + 2e^{-i\omega} - e^{-i2\omega}}{2\sqrt{2}}. \end{aligned} \qquad (3)$$

3. TRIANGULAR BIORTHOGONAL WAVELETS

Discrete signals are naturally indexed by integers in one-dimension, but the indexing may become a nontrivial problem in dimensions more than one. We find it convenient to employ the primitive translation vectors used in solid state physics in classifying crystal structures, see e.g., [10]. In two-dimensional plane, we define two primitive translation vectors

$$\boldsymbol{t}_1 = \begin{pmatrix} 1 \\ 0 \end{pmatrix}, \quad \boldsymbol{t}_2 = \begin{pmatrix} -\frac{1}{2} \\ \frac{\sqrt{3}}{2} \end{pmatrix}.$$

For notational convenience we also define $\boldsymbol{t}_3 = -\boldsymbol{t}_1 - \boldsymbol{t}_2$ and $\boldsymbol{t}_0 = \boldsymbol{0}$. The regular triangular Bravais lattice is defined by

$$\Lambda = \{\boldsymbol{t} = n_1\boldsymbol{t}_1 + n_2\boldsymbol{t}_2 | (n_1, n_2) \in \mathbb{Z}^2\}.$$

The domain containing all the points whose closest site is a given site $\boldsymbol{t} \in \Lambda$ is the Wigner-Seitz cell of the site. In our regular triangular lattice Λ, the Wigner-Seitz cell is a hexagon, which plays the role of a pixel of an image. The vectors $\boldsymbol{t}_m$, $m = 1, 2, 3$, the Bravais lattice Λ, and the Wigner-Seitz cell are shown in Figure 1 (left). The reciprocal lattice vectors are defined by

$$\boldsymbol{\lambda}_1 = \begin{pmatrix} 0 \\ \frac{2}{\sqrt{3}} \end{pmatrix}, \quad \boldsymbol{\lambda}_2 = \begin{pmatrix} 1 \\ \frac{1}{\sqrt{3}} \end{pmatrix},$$

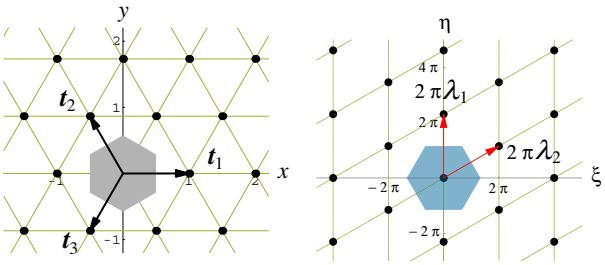

Figure 1: The primitive translation vectors, Bravais lattice, and the Wigner-Seitz cell (left), the reciprocal lattice vectors, reciprocal lattice, and the Brillouin zone (right)

and $\boldsymbol{\lambda}_3 = \boldsymbol{\lambda}_1 + \boldsymbol{\lambda}_2$. They generate the reciprocal lattice

$$\widehat{\Lambda} = \{2\pi(\boldsymbol{\lambda} = m_1\boldsymbol{\lambda}_1 + m_2\boldsymbol{\lambda}_2) | (m_1, m_2) \in \mathbb{Z}^2\}.$$

The Wigner-Seitz cell of the reciprocal lattice $\widehat{\Lambda}$ is the Brillouin zone. The vectors $2\pi\boldsymbol{\lambda}_m$, $m = 1, 2$, the reciplocal lattice $\widehat{\Lambda}$, and the Brillouin zone are shown in Figure 1 (right).

The LP filter $\{h[\boldsymbol{t}]\}_{\boldsymbol{t}\in\Lambda}$ is now defined on the Bravais lattice Λ, and let

$$\hat{h}(\boldsymbol{\omega}) = \sum_{\boldsymbol{t}\in\Lambda} h[\boldsymbol{t}]\, e^{-i\boldsymbol{\omega}\cdot\boldsymbol{t}}, \quad \boldsymbol{\omega} \in \mathbb{R}^2.$$

Since $\hat{h}(\boldsymbol{\omega})$ is periodic with respect to the translation $\boldsymbol{\omega} \to \boldsymbol{\omega} + 2\pi\boldsymbol{\lambda}$, one of the Brillouin zones is its defining domain. A crucial observation is that all the sites of Λ may be classified into four independent sublattices

$$\Lambda_m = \{2\boldsymbol{t} + \boldsymbol{t}_m | \, \boldsymbol{t} \in \Lambda\}, \quad m = 0, 1, 2, 3,$$

which play the role of even and odd indices in one dimension. Accordingly, the filter may be represented as the sum of the corresponding components

$$\hat{h}_m(\boldsymbol{\omega}) = \sum_{\boldsymbol{t}\in\Lambda} h[2\boldsymbol{t} + \boldsymbol{t}_m]e^{-i\boldsymbol{\omega}\cdot\boldsymbol{t}}, \quad m = 0, 1, 2, 3.$$

The signal $\{c_j[\boldsymbol{t}]\}_{\boldsymbol{t}\in\Lambda}$ is also assumed to be given on the Bravais lattice Λ. Let

$$\hat{c}_j(\boldsymbol{\omega}) = \sum_{\boldsymbol{t}\in\Lambda} c_j[\boldsymbol{t}]\, e^{-i\boldsymbol{\omega}\cdot\boldsymbol{t}},$$

then it is decomposed into four independent components

$$\hat{c}_{m,j}(\boldsymbol{\omega}) = \sum_{\boldsymbol{t}\in\Lambda} c_j[2\boldsymbol{t} + \boldsymbol{t}_m]\, e^{-i\boldsymbol{\omega}\cdot\boldsymbol{t}}, \quad m = 0, 1, 2, 3.$$

As in (1), the decomposition is represented as

$$\begin{pmatrix} \hat{c}_{j-1}(\boldsymbol{\omega}) \\ \hat{d}_{1,j-1}(\boldsymbol{\omega}) \\ \hat{d}_{2,j-1}(\boldsymbol{\omega}) \\ \hat{d}_{3,j-1}(\boldsymbol{\omega}) \end{pmatrix} = \widehat{P}(\boldsymbol{\omega})^\dagger \begin{pmatrix} \hat{c}_{0,j}(\boldsymbol{\omega}) \\ \hat{c}_{1,j}(\boldsymbol{\omega}) \\ \hat{c}_{2,j}(\boldsymbol{\omega}) \\ \hat{c}_{3,j}(\boldsymbol{\omega}) \end{pmatrix}, \qquad (4)$$

where $\widehat{P}(\boldsymbol{\omega})^\dagger$ is the Hermitian conjugate of the 4×4 polyphase matrix. Note that there are three detail components $\hat{d}_{m,j-1}(\boldsymbol{\omega})$,

$m = 1, 2, 3$. We now wish to extend the polyphase matrix (2) to this case, which is found to be

$$\widehat{P}(\omega)^{\dagger} = \begin{pmatrix} 2 & 0 & 0 & 0 \\ 0 & \frac{1}{2} & 0 & 0 \\ 0 & 0 & \frac{1}{2} & 0 \\ 0 & 0 & 0 & \frac{1}{2} \end{pmatrix} \begin{pmatrix} 1 & \hat{u}_1 & \hat{u}_2 & \hat{u}_3 \\ 0 & 1 & 0 & 0 \\ 0 & 0 & 1 & 0 \\ 0 & 0 & 0 & 1 \end{pmatrix} \begin{pmatrix} 1 & 0 & 0 & 0 \\ -\hat{p}_1 & 1 & 0 & 0 \\ -\hat{p}_2 & 0 & 1 & 0 \\ -\hat{p}_3 & 0 & 0 & 1 \end{pmatrix} \begin{pmatrix} 1 & 0 & 0 & 0 \\ 0 & -1 & 1 & 1 \\ 0 & 1 & -1 & 1 \\ 0 & 1 & 1 & -1 \end{pmatrix} \tag{5}$$

with three predictors $\hat{p}_m(\omega)$ and updaters $\hat{u}_m(\omega)$, $m = 1, 2, 3$. We define the dual polyphase matrix as $\widehat{\widetilde{P}}(\omega) = \widehat{P}(\omega)^{\dagger^{-1}}$, then the perfect reconstruction condition

$$\widehat{\widetilde{P}}(\omega)\,\widehat{P}(\omega)^{\dagger} = I \tag{6}$$

is guaranteed. In particular, its upper left component implies

$$\hat{\tilde{h}}(\omega)\,\hat{h}^*(\omega) + \sum_{m=1}^{3} \hat{\tilde{g}}_m(\omega)\,\hat{g}_m^*(\omega) = 4 \tag{7}$$

corresponding to the halfband condition in one dimension. The orthogonal case of (7) has been obtained in [11].

Once the filters are found, the two-dimensional scaling functions $\phi(\boldsymbol{r})$ and wavelets $\psi_m(\boldsymbol{r})$, $m = 1, 2, 3$, $\boldsymbol{r} \in \mathbb{R}^2$, are defined by their Fourier transform,

$$\hat{\phi}(\omega) = \prod_{j=1}^{\infty} \frac{1}{2}\hat{h}\Big(\frac{\omega}{2^j}\Big), \quad \hat{\psi}_m(\omega) = \frac{1}{2}\hat{g}_m\Big(\frac{\omega}{2}\Big)\hat{\phi}\Big(\frac{\omega}{2}\Big), \quad \omega \in \mathbb{R}^2.$$

We do not further consider these functions, and concentrate on the properties of the filters. We now proceed to some examples.

3.1 Triangular Haar Filter

The simplest choice is

$$\hat{p}_m(2\omega) = 1, \quad \hat{u}_m(2\omega) = \frac{1}{4}.$$

Then we find the triangular Haar filter

$$\begin{pmatrix} \hat{h}(\omega) \\ \hat{g}_1(\omega) \\ \hat{g}_2(\omega) \\ \hat{g}_3(\omega) \end{pmatrix} = \begin{pmatrix} \hat{\tilde{h}}(\omega) \\ \hat{\tilde{g}}_1(\omega) \\ \hat{\tilde{g}}_2(\omega) \\ \hat{\tilde{g}}_3(\omega) \end{pmatrix} = \frac{1}{2}\begin{pmatrix} 1 & 1 & 1 & 1 \\ -1 & -1 & 1 & 1 \\ -1 & 1 & -1 & 1 \\ -1 & 1 & 1 & -1 \end{pmatrix} \begin{pmatrix} 1 \\ e^{-i\omega\cdot\boldsymbol{t}_1} \\ e^{-i\omega\cdot\boldsymbol{t}_2} \\ e^{-i\omega\cdot\boldsymbol{t}_3} \end{pmatrix},$$

which is orthogonal. As our preliminary studies show [14], the energy is evenly distributed over three detail decomposed components, implying that isotropy of images is respected. We do not consider this filter further here.

3.2 Triangular Linear Prediction Filter

If we choose

$$\hat{p}_m(2\omega) = \frac{1 + e^{i2\omega\cdot\boldsymbol{t}_m}}{2}, \quad \hat{u}_m(2\omega) = \frac{1 + e^{-i2\omega\cdot\boldsymbol{t}_m}}{8}, \tag{8}$$

we have the triangular version of CDF(2,2) filter (3). We display the filter coefficients and the Fourier transform in Figure 2–5. The filters $\hat{g}_m(\omega)$, $m = 1$ and 3 are simply $\pm 2\pi/3$ rotations of the $m = 2$ case. As we see in the frequency

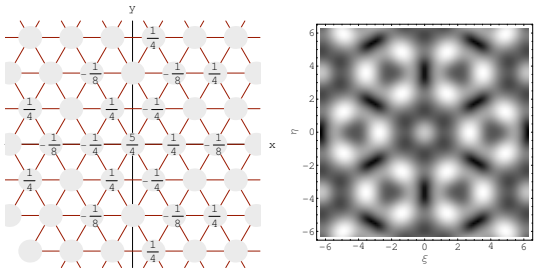

Figure 2: The LP filter coefficients $h[\boldsymbol{t}]$ and $|\hat{h}(\omega)|$

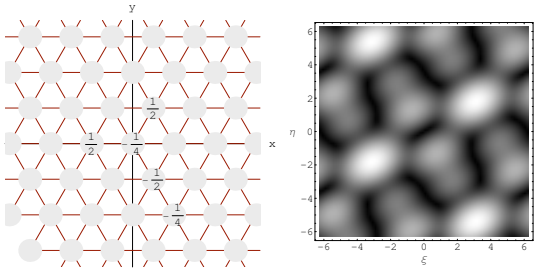

Figure 3: The HP filter coefficients $g_2[\boldsymbol{t}]$ and $|\hat{g}_2(\omega)|$

response along the $\boldsymbol{\lambda}_1$ direction in Figure 6, the sum in (7) consists of low pass, high pass and band pass combinations

$$\begin{aligned}
\hat{\tilde{h}}(\omega\boldsymbol{\lambda}_1)\,\hat{h}^*(\omega\boldsymbol{\lambda}_1) &= 1 + \frac{5\cos\omega}{4} + \frac{11}{16}\cos 2\omega + \frac{11}{16}\cos 3\omega \\
&\quad + \frac{1}{4}\cos 4\omega + \frac{1}{16}\cos 5\omega + \frac{1}{16}\cos 6\omega, \\
\hat{\tilde{g}}_1(\omega\boldsymbol{\lambda}_1)\,\hat{g}_1^*(\omega\boldsymbol{\lambda}_1) &= \frac{11}{8} - \frac{17\cos\omega}{8} + \frac{3}{4}\cos 2\omega + \frac{1}{8}\cos 3\omega \\
&\quad - \frac{1}{8}\cos 4\omega, \\
\sum_{m=2}^{3} \hat{\tilde{g}}_m(\omega\boldsymbol{\lambda}_1)\,\hat{g}_m^*(\omega\boldsymbol{\lambda}_1) &= \frac{13}{8} + \frac{7\cos\omega}{8} - \frac{23}{16}\cos 2\omega - \frac{13}{16}\cos 3\omega \\
&\quad - \frac{1}{8}\cos 4\omega - \frac{1}{16}\cos 5\omega - \frac{1}{16}\cos 6\omega.
\end{aligned}$$

Note that near the alias point $\omega \approx \pi\boldsymbol{\lambda}_1$,

$$\hat{\tilde{h}}(\omega\boldsymbol{\lambda}_m)\,\hat{h}^*(\omega\boldsymbol{\lambda}_m) \propto (\omega - \pi)^4,$$

which implies that the filter is of order (2, 2).

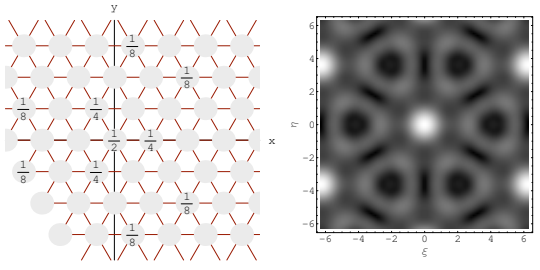

Figure 4: The dual filter coefficients $\tilde{h}[\boldsymbol{t}]$ and $|\hat{\tilde{h}}(\omega)|$

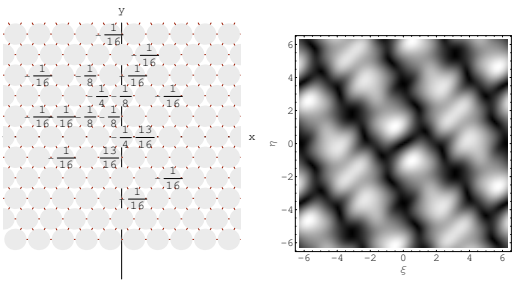

Figure 5: The dual filter coefficients $\tilde{g}_2[\boldsymbol{t}]$ and $|\hat{\tilde{g}}_2(\omega)|$

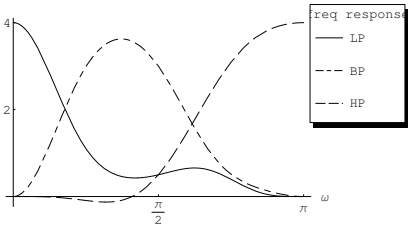

Figure 6: The frequency response of the filters

3.3 Generalization to Higher Orders

In (8), if we choose

$$\hat{u}_m(\omega) = \frac{-3e^{i\omega\cdot\boldsymbol{t}_m} + 19 + 19e^{-i\omega\cdot\boldsymbol{t}_m} - 3e^{-i2\omega\cdot\boldsymbol{t}_m}}{16}, \qquad (9)$$

we have the triangular version of CDF(2,4) filter (3). This shows that our method is general so that filters of higher order may be obtained. However, we do not discuss general case here, and we demonstrate that decomposed images respect isotropy with the triangular linear prediction filters constructed in Subsection 3.2.

4. ISOTROPY IN IMAGE PROCESSING

We now wish to see that the wavelet transform respects isotropy of images. However, our triangular filters are designed to deal with two-dimensional data defined on the regular triangular Bravais lattice, which is not the standard format; image data are usually rectangular arrays of numbers. To deal with this difference in our preliminary study of isotropy, we consider that the second primitive translation vector $\boldsymbol{t}_2$ is rotated clockwise to approach the y axis. Then, the hexagonal Wigner-Seitz cells will be deformed to form nearly rectangular arrays, as shown in Figure 7. We treat image data as the original signal $\{c_j[\boldsymbol{t}]\}$, and decomposed images $\{c_{j-1}[\boldsymbol{t}]\}$, and $\{d_{j-1}[\boldsymbol{t}]\}$, $\boldsymbol{t} \in \Lambda$, in this limit. We compare the decomposition of sample images by our triangular linear prediction filter (TriDWT), with the images of wavelet transform in the tensor product transform (TensorDWT). Since the filters are biorthogonal in all cases, we compute the primal and dual transforms, which is used to obtain the energy of coarse and detail components.

We consider the upper right quarter of concentric circles as an example of axially symmetric artificial images, and Lena image as an example of natural images. Figure 8–9 show the decomposed images. The upper left block is the result of primal TensorDWT, and upper right block is that of

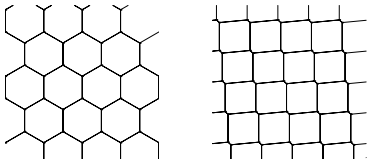

Figure 7: The honeycomb and nearly square array of Wigner-Seitz cells

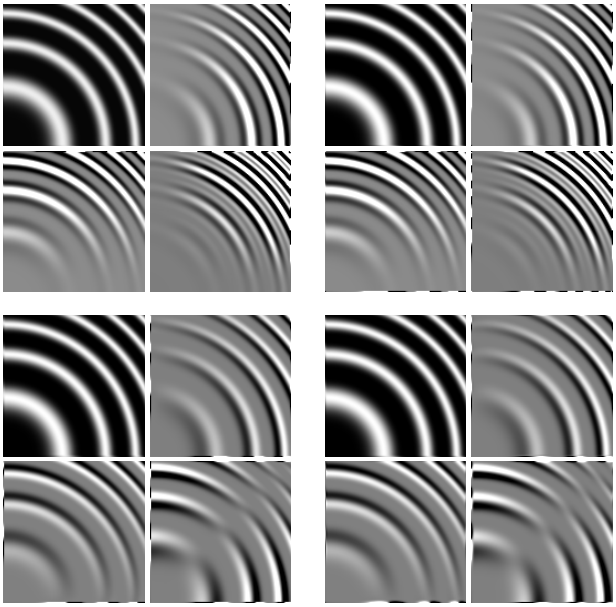

Figure 8: Decomposed images of concentric circles. (Upper row is tensor primal and tensor dual, bottom row is triangular primal and triangular dual)

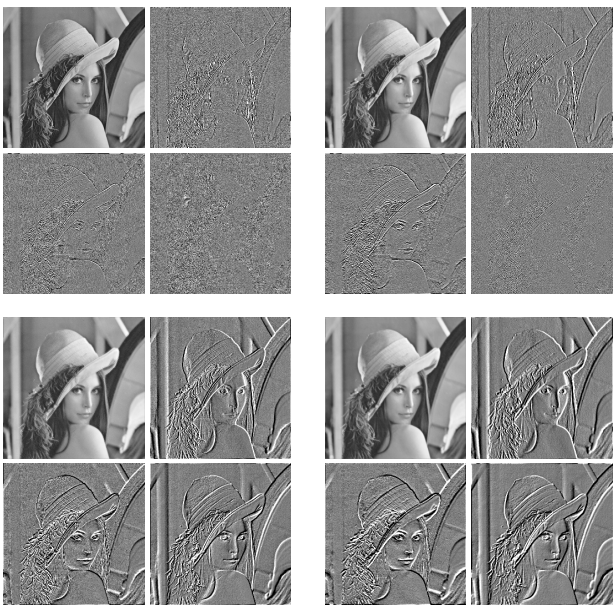

Figure 9: Decomposed images of Lena image. (Upper row is tensor primal and tensor dual, bottom row triangular primal and triangular dual

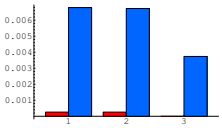

Figure 10: Energy distribution over the three detail components of concentric circles. (red or left side of each column corresponds to tensor product transform, and blue or right side corresponds to triangular transform)

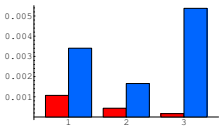

Figure 11: Energy distribution over the three detail components of Lena image, in the same format as in Figure 10.

dual TensorDWT. In each block, the LL, LH, HH, and HL components clockwise from the upper left image. The lower left block is the result of primal TriDWT, and the lower right block is that of dual TriDWT. In each block, the coarse, and the three detail components are placed clockwise from the upper left image. Note that the values of each image data are normalized within each image. If the values would be normalized in each block of four images, the detail images would be invisible. In Figure 10–11, we show how the energy is distributed over the detail components.

From these figures, we have the following observations.

- More portion of the total energy goes to the three detail components in TriDWT.
- Energy is more evenly distributed over the three detail components in TriDWT, while in TensorDWT the portion of the energy of HH components is appreciably less than all the other components.
- The detail components of TriDWT extract the edge structure of Lena image well.

All the observations indicate that isotropy of images is well respected in TriDWT.

5. CONCLUSION AND FURTHER STUDIES

A method of constructing new non-separable biorthogonal wavelet filters defined on the regular triangular lattice is proposed. Using the triangular version of the CDF(2,2) filter, the filter coefficients, and their structure in the Fourier domain are displayed. They are applied to two sample images, whose results indicate that wavelet transform appears to respect isotropy of images well. We summarize the features of the triangular wavelet filters.

- Filters of an arbitrary order can be constructed.
- All the filter coefficients can be made real exact fraction, and the number of coefficients is relatively small.
- Due to the use of lifting, computational cost of DWT is not large.

In summary, our triangular wavelet filters appear to have many nice features. While definite statements can be made only after thorough investigations, which is currently under study, our new triangular filters appear promising.

The authors would like to thank the referees for valuable suggestions to improve the paper. One of the authors (S.S.) would like to thank his graduate student K. Fujinoki for fruitful discussions. He is also grateful to his family, and Dr. Yoshizawa and the nurses of Nippon Medical School Chiba Hokusoh Hospital for full support, where the final version of this paper is written.

REFERENCES

[1] S. Mallat, *A wavelet tour of signal processing*, 2nd ed., Academic Press, 2001.

[2] J. Kovačević and M. Vetterli, "Nonseparable multidimensional perfect reconstruction filter banks and wavelet bases for $\mathbb{R}^n$," *IEEE Trans. Information Theory*, vol.38(2), 533–555, 1992.

[3] N. Kingsbury, "The dual-tree complex wavelet transform: a new technique for shift invariance and directional filters," *Proc. 8th IEEE DSP Workshop*, paper no.86, 1998.

[4] H. Kawabata, H. Toda, Z. Zhang, and H. Fujiwara, "A new complex wavelet transform by using RI-spline wavelet," in *Proc. IEEE Int. Conf. Acoust., Speech, Signal Processing*, Montreal, May 2004, vol.2, pp.937–940.

[5] W. Sweldens, "The lifting scheme: a custom-design construction of biorthogonal wavelets," *Applied and Computational Harmonic Analysis*, vol. 3(2), pp. 186–200, 1996.

[6] W. Sweldens, "The lifting scheme: A Construction of second generation wavelets," *SIAM J. Math. Anal.*, 29(2), 511–546, 1997.

[7] P. Schröder and W. Sweldens, "Sperical wavlets: efficiently representing functions on the sphere," *Computer Graphics Proceedings (SIGGRAPH 95)*, 161–172, 1995.

[8] I. Daubechies, I. Guskov, P. Schröder, and W.Sweldens, "Wavelets on Irregular Point Sets," *Phil. Trans. R.Soc.Lon.A.*, vol.357(1760), 2397–2413, 2000.

[9] A. Cohen, I. Daubechies, and J. Feauveau, "Biorthogonal Bases of Compactly supported Wavelets," *Comm. Pure Appl. Math.*, vol.45, 486–560, 1992.

[10] G. Grosso and G. P. Parravicini, *Solid State Physics*, Elsevier Academic Press, 2000.

[11] E. P. Simonchelli, and E. H. Adelson, "Non-Separable Extensions of Quadrature Mirror Filters in Multiple Dimensions," *Proceedings of the IEEE*, vol.78(4), 652–664, 1990.

[12] E. P. Simonchelli, W. T. Freeman, E. H. Adelson and D. J. Heeger , "Shiftable Multiscale, Transforms," *IEEE Trans. Information Theory*, vol.38(2), 587–607, 1992.

[13] S. Sakakibara, "Aspects of Wavelet Analysis," *Proceedings of Sice2005, International Conference on Instrumentation, Control and Information Technology*, Okayama University, Okayama, Japan, August 8–10, paper no. MP1-03-5, 2005.

[14] K. Fujinoki and S. Sakakibara, "Triangular Wavelet Basis and its Application," *Proceedings of Sice2005, International Conference on Instrumentation, Control and Information Technology*, Okayama University, Okayama, Japan, August 8–10, paper no. MP1-03-4, 2005.